Static and fatigue experimental tests on a full scale fuselage panel and FEM analyses

Raffaele Sepe, Enrico Armentani
Department. of Chemical, Materials and Production Engineering - University of Naples Federico II, P.le V. Tecchio, 80 - 80125 Naples, Italy.
raffsepe@unina.it

Francesco Caputo
Department of Industrial and Information Engineering - Second University of Naples
Via Roma 29 - 81031 Aversa, Italy.

ABSTRACT. A fatigue test on a full scale panel with complex loading condition and geometry configuration has been carried out using a triaxial test machine. The demonstrator is made up of two skins which are linked by a transversal butt-joint, parallel to the stringer direction. A fatigue load was applied in the direction normal to the longitudinal joint, while a constant load was applied in the longitudinal joint direction. The test panel was instrumented with strain gages and previously quasi-static tests were conducted to ensure a proper load transferring to the panel. In order to support the tests, geometric nonlinear shell finite element analyses were conducted to predict strain and stress distributions. The demonstrator broke up after about 177000 cycles. Subsequently, a finite element analysis (FEA) was carried out in order to correlate failure events; due to the biaxial nature of the fatigue loads, Sines criterion was used. The analysis was performed taking into account the different materials by which the panel is composed. The numerical results show a good correlation with experimental data, successfully predicting failure locations on the panel.

KEYWORDS. Multiaxial fatigue; Full scale panel; FE model; Sines criterion; Life prediction.

INTRODUCTION

The global risk analysis must take into account all statistical structural parameters, their variation and their effects on design and response properties of aircraft structural components. In fact the structural safety and reliability can be estimate on a probabilistic basis providing information on the confidence that should be given to the predicted behaviour. The development of an overall probabilistic approach, aim of to evaluate the damage tolerance of the structure, must be based on a better description of the entire process of structural degradation (i.e. as crack initiation process, the use of initial flaw sizes, crack growth in small and long crack regime, residual strength) tuned to different structural details. Therefore one of the main tasks of the airframe design is the full-scale fatigue test, where an airframe is subjected to realistic loads, which are representative of those predicted to occur over the life type. Generally these fatigue tests are cycled until the equivalent of several lifetimes is achieved or an unrepairable failure occurs. In the last years several full scale fatigue tests on fuselage panels have been conducted [1-5]. In these tests the airframe is subjected to

loads of varying amplitude and complexity for a specified period of testing in order to simulate the fatigue loads that are predicted to occur over the life of the airframe. The main aim of the full scale test is to produce fatigue damage, that may be expected during service, in order to discover where fatigue cracking may occur and to assess its behaviour.
Together with the experimental activity, in the last 20 years, the finite element method has been further developed and now represents a useful tool in the numerical evaluation of local stress and strain; the results obtained can be used to carry out both fatigue strength and a damage tolerant assessment. Cordes [6] predicts fatigue cycles from stress/strain data, a calculated crack-tip energy, and a calculated fracture toughness. Grbovic and Rasuo [7] show that it is possible, by using finite element analysis (FEA), to obtain not only the good estimation of the fatigue life of the assembly such as the spar of the light aircraft, but also a good prediction of a number of load cycles which will propagate a crack on the spar to a certain length. Šedek et al. [8] evaluate the crack growth in an unstiffened and integrally stiffened wing panel without and with retardation effect evaluation. Crack growth predictions are performed by using both the linear damage accumulation principle and the FASTRAN retardation model. Furukawa et al. [9] a new methodology for modeling fatigue crack propagation in pressurized cylindrical shell structures. The methodology involves the evaluation of four stress intensity factors that are used to characterize cracked shell structures, the determination of the crack propagation trajectory as an integral part of the simulation process, and the prediction of the load cycles needed for the crack to propagate from its initial length until the final crack length. In addition, the numerical analyses make it possible to study the fatigue and damage tolerant behaviour of complex structures using fracture mechanics approach [10-12]. Moreover, in order to determine an acceptable fatigue life for the joint structures or to develop an effective riveted reinforcement methodology an extensive research has been conducted in the area of riveted patch joint performance: the majority of numerical analyses have been performed using the Finite Element Method (FEM), but some work has also been done using the Dual Boundary Element Method (DBEM) [13-15].
This paper reports the results of extended fatigue testing of a fuselage panel using a full-scale aircraft structural testing machine. The test panel was instrumented with strain gages, and previously quasi-static tests were conducted to ensure a proper load transfer to the panel. To support these tests, geometric nonlinear shell finite element analyses were conducted to predict strain and stress distributions and other parameters governing the crack initiation. The FE model allows to reproduce the effective shape and conditions of the specimen tested; moreover, it gives a complete description of the state of strain and stress in the whole panel. Crack formation during the fatigue test was monitored at every 10˙000 cycles using high-magnification visual inspection. After 164˙292 cycles a crack appeared on the panel frame, successively growing up and leading to several failures. After 12˙708 cycles more the panel broke down definitively at the middle-lower bay, near the third frame. Subsequently, a finite element analysis was carried out to correlate failure events; due to the actual biaxial nature of the fatigue loads, Sines criterion was used. The analysis was performed taking into account the different materials of which the panel is composed. The output shows a good correlation between experimental data and numerical results, that successfully may predict the failure locations on the panel.

EXPERIMENTAL TEST

Test description

The full scale aeronautical test panel is shown in Fig. 1. The panel, whose sizes are 2181x2181 mm² (excluding the aluminum gripping plates), consists of two panels with the thickness of 1.2 mm, four frames and thirteen stringers. Stringers are connected to the frames with stringer clips. The frames are connected to the skins by shear ties.
The lower and upper panel skins are joined by a lap transversal joint that is parallel to the stringer direction. The upper and lower skins are made of Al 2024-T3, the stringers, frames, shear ties and stringer clips are made of Al 7075-T6 51. The tested panel has been instrumented by strain gages, that are located on the internal side of the panel. Seven strain gages type CEA-13-250UW-350 of MM Vishay were bonded on the specimen. The strain gauges S1, S2, S4, S6, S7 (Fig. 2) measure the strains on the skin, while those S3 and S5 measure strains on lower pad of central frames. S2, S3, S4, S5, S6 provide strains in longitudinal direction of the panel, while S1 and S7 provide strains in transversal direction. The strain gages were bonded by a two-component epoxy adhesive in order to ensure good performance in case of large strains and each strain gage was attached to an acquisition system through a quarter bridge linkage. The positioning coordinates (X, Y, Z) of the strain gages are reported in Tab. 1.
Some interesting machines were designed and manufactured in the past [16-19], but they seem to be able to apply only limited loading conditions on reduced scale specimens. Three loading axes, one diagonal, and two normal with respect to the side of the panel, have to be necessary to simulate correctly the structural behaviour of an aircraft fuselage, where the

normal stresses due to the internal pressurization are comparable with the shear stress due to external loads. Moreover full-scale panels should be tested to investigate on structural buckling phenomena depending on specimen conformation.

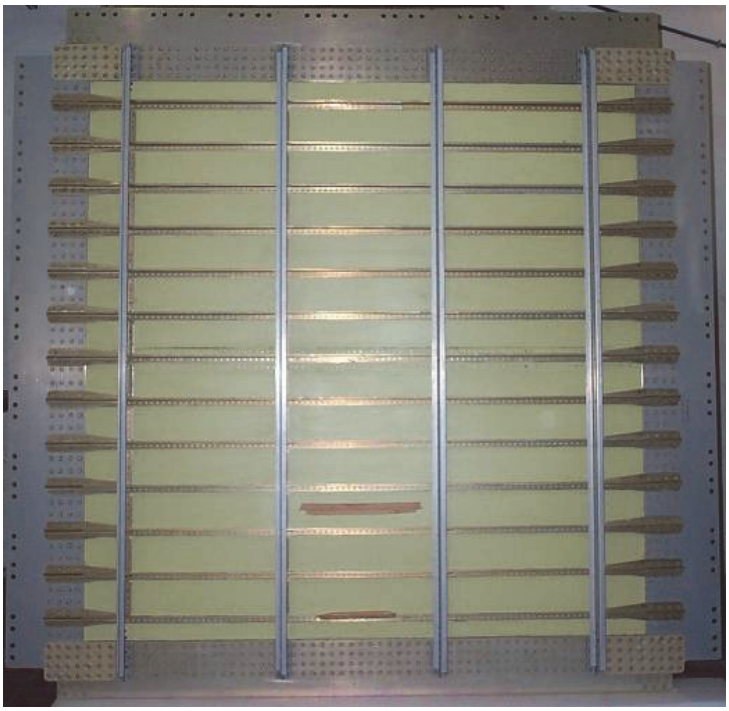

Figure 1: Test panel.

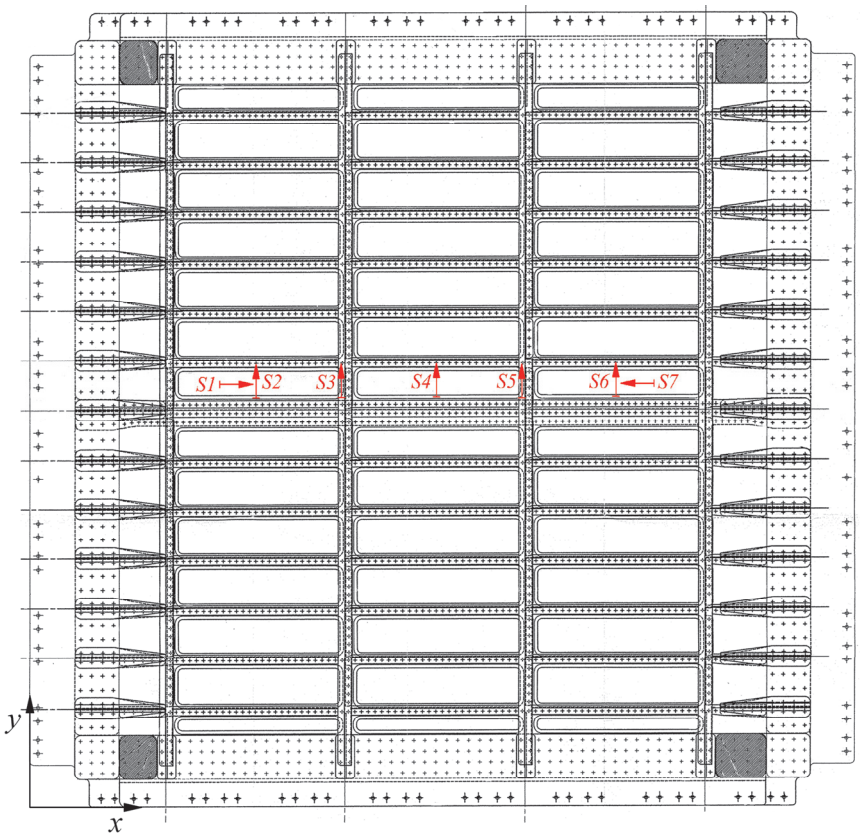

Figure 2: Strain gages layout.

Coordinates	Strain gauges						
	S1	S2	S3	S4	S5	S6	S7
X [mm]	680	710	995	1235	1525	1770	1800
Y [mm]	1144	1144	1144	1144	1144	1144	1144
Z [mm]	1.2	1.2	38	1.2	38	1.2	1.2

Table 1: Strain gages positions on panel (see reference system in Fig. 2).

The test machine used to test the full scale aeronautical test panel is shown in Fig. 3. Such machine consists of five hydraulic cylinders, one in of the diagonal direction and the other four aligned along two orthogonal directions, hinged onto supports rigidly connected to an octagonal box frame. In the diagonal direction the maximum load is 1000 kN, while in the normal directions it is respectively 250 kN in X direction and 500 kN in Y direction (for the reference system see Fig. 2). Its overall sizes are about 5000x5000x2000 mm^3, without considering the hydraulic and electric control units. The machine is able to test flat specimens up to an extension of 2500x2500 mm^2, including the gripping zone.

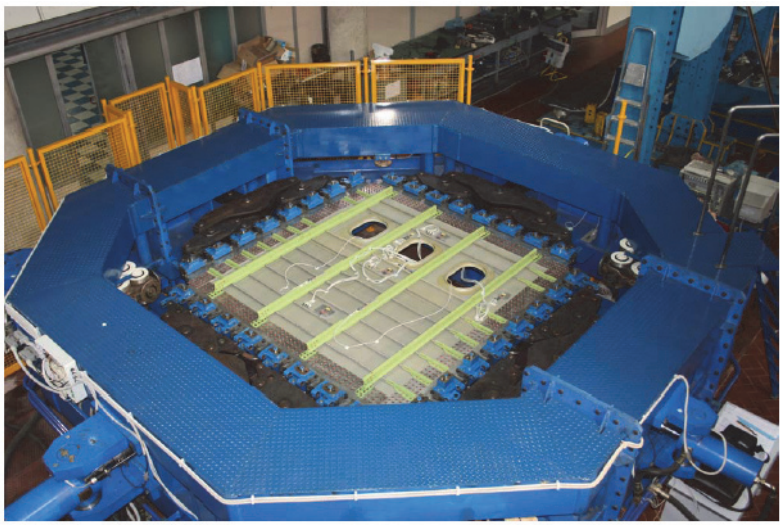

Figure 3: Tested panel loaded by the multi-axial full scale fatigue machine.

The gripping system consists of 32 items, 8 for each specimen side; this localized loading practically determines the required stress distribution on the specimen side. Each grip transfers the load to the specimen by friction and by four special shaped pins (Fig. 4).
The four traction cylinders are connected to the 8 grips by a rocker arm balancing system. The levers have equal arms, so the cylinder load is uniformly distributed; it would be possible to apply a different load distribution on specimen side with a non equal arm lever system. Moreover the localized grips and the balancing system allow free panel side elongations.
The diagonal cylinder applies the shear load by means of a rope winded up to 128 pulleys. Some pulleys are assembled on the grips and some others are assembled on a plate linked to the cylinder as shown in Fig. 5. Two pulleys for one grip, in symmetric position with regard to the panel, avoid non expected moments. The pulleys are different in diameter and vertical position to avoid interference with the rope. They can rotate to balance different rope length elongations. Just two locked rope pieces are used, one for two consecutive panel sides.
A rolling bearing system ensures the "simply supported edges" boundary condition. It allows the in plane specimen translations and prevents the out of plane one. This system is supported by a secondary frame connected to the principal one. The secondary frame reacts to out of plane forces that can arise by geometric and material asymmetry or by buckling phenomena. Moreover the machine is not constrained by an external bed because it is entirely balanced. The cylinder

displacements and the applied loads are measured respectively by linear position transducers and load cells, located along the cylinder axes. Both this devices generate analogical signals accepted by control system.

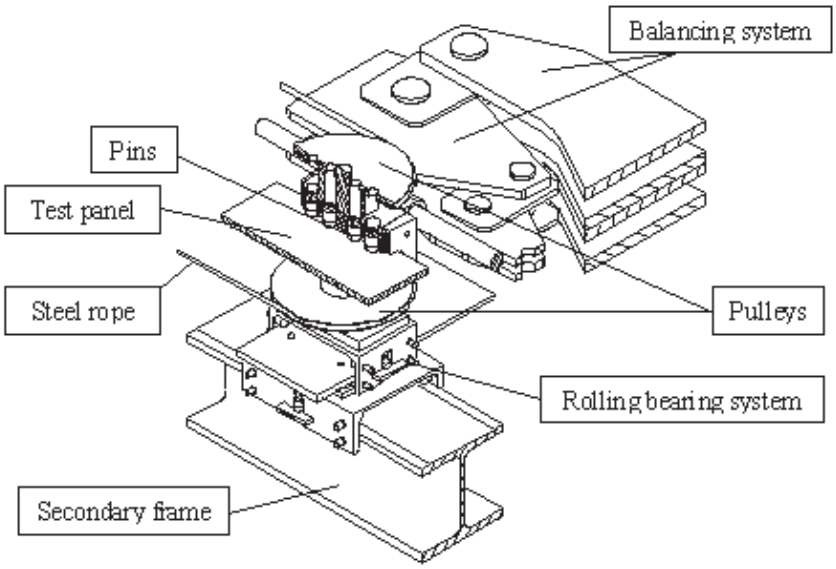

Figure 4: Mechanical components of the machine.

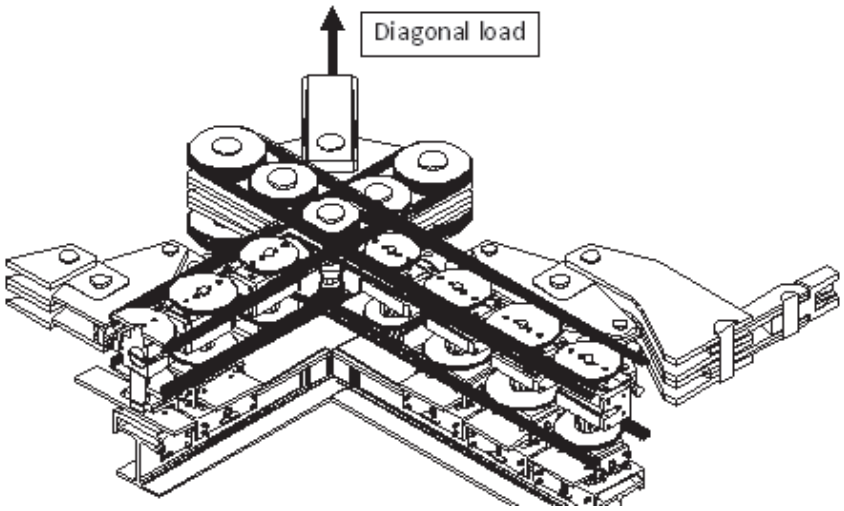

Figure 5: Shear load introduction system.

Test procedure

Four types of load controlled tests have been carried out:

- T1: Mono-axial static test - P_y = 400 kN, with loads applied with a ramp of 1 kN/sec;
- T2: Mono-axial static test - P_x = 250 kN, with loads applied with a ramp of 0.62 kN/sec;
- T3: Bi-axial static test - P_x = 250 kN and P_y = 400 kN, with loads applied with a ramp of 0.62 kN/sec in X direction and of 1 kN/sec in Y direction;
- T4: Fatigue test - A fatigue load P_{ymax} = 400 kN, (frequency equal to 1 Hz) has been applied in the normal direction to the longitudinal joint with a load ratio R = 0.01 while a static load P_x = 200 kN has been applied in the joint direction.

During fatigue test visual inspections were carried out every 10˙000 cycles. No cracks were found in the joint region during the test. The first significant failure was detected at 164˙292 cycles. This failure initiated in a hole of the web of one of the frames as shown Figs. 6 and 7. The cracks were easily visible with the unaided eye and were located approximately half-length of the frame. The extension of the crack to the size shown occurred in a single cycle. Note that, while the three undamaged frames continued to transmit load, the failed frame did not. Immediately following the failure of the frame,

the panel was statically tested with loading condition T1. Then the fatigue test is continued and other 12˙708 cycles were applied and then the demonstrator broke down definitively at the middle-lower bay, near the third frame (Fig. 8).

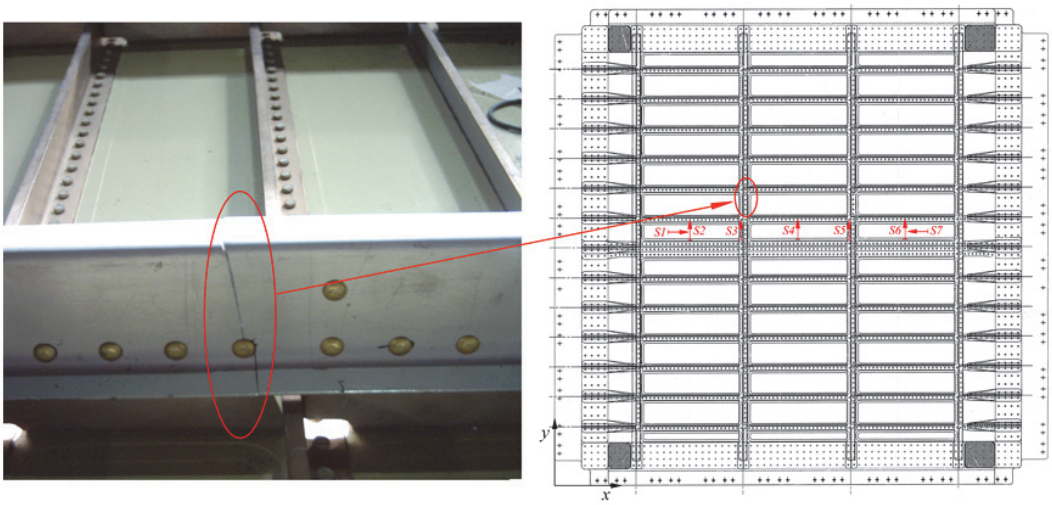

Figure 6: Frame failure at 164˙292 cycles.

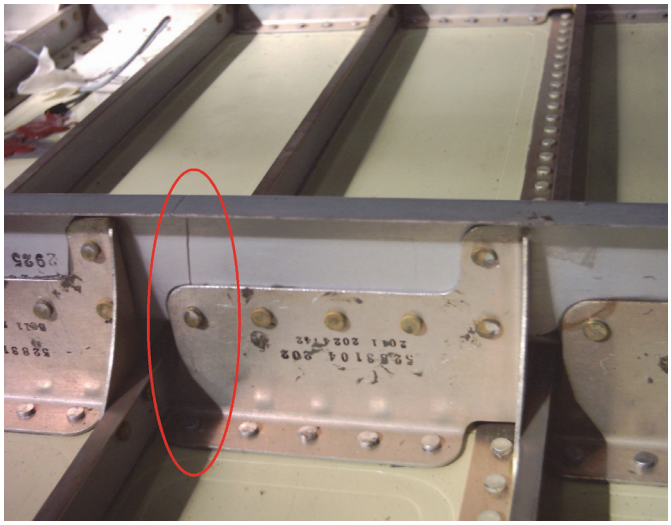

Figure 7: Frame failure at 164˙292 cycles (detail).

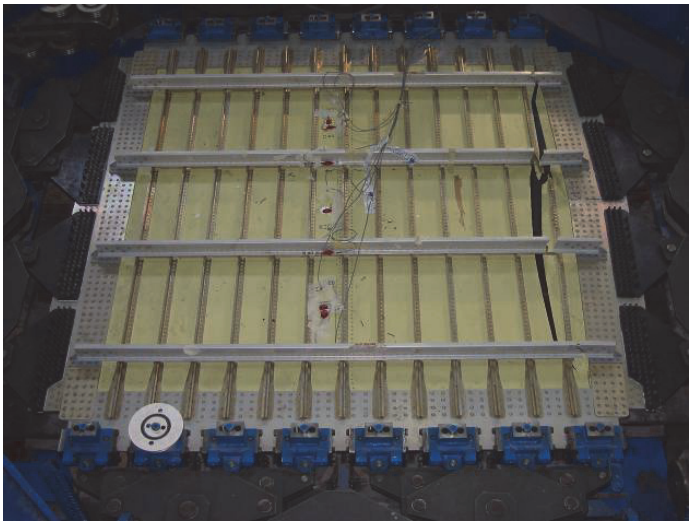

Figure 8: Final failure at 177000 cycles.

FE ANALYSIS

Geometric nonlinear finite element analyses were conducted to predict the strain and stress distributions for the several test condition. The analyses were carried out by using a commercially available finite element code (ANSYS). The panel was modeled using two-dimensional four-nodes shell elements (SHELL 181) with each node having six degrees of freedom for each node. A global view of the finite element model is shown in Fig. 9, which consists of 64432 elements and 205664 nodes; here different colors of shell elements are associated to different thicknesses. Four-noded shell elements were used throughout to model skin, frames, stringer clips, stringers, and load attachment doublers. The presence of the rivets was taken into account defining the proper number and location of constraint points (CP). The analysis has been performed in geometric non linear condition (large displacements), while the material has been considered in linear elastic hypothesis with Young modulus equal to 72500 MPa for Al 2024-T3 aluminium alloy and 71016 MPa for Al 7075-T6 51 aluminium alloy, and Poisson's ratio is equal to 0.33 for both materials. Stress stiffening capability is included.

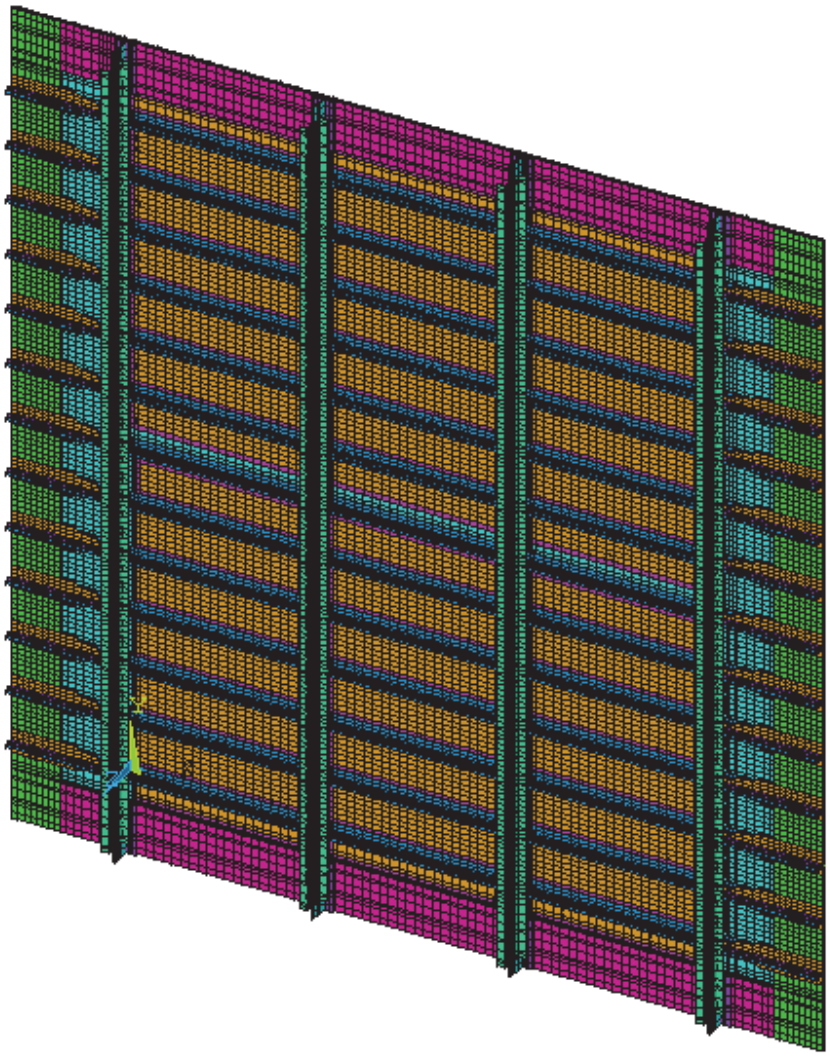

Figure 9: FE model of the panel.

Sines criterion

Experimental investigations in last years have provided numerous hypotheses on the Multiaxial High-Cycle Fatigue criteria. In literature, many proposals of such criteria can be found [20-28]. From a numerical point of view, the criteria which may be conveniently applied are of two types: criteria based on stress state invariants and criteria using average stresses or deformations in an elementary volume. In 1959, Sines [29] reviewed the results of experiments on the effect of different combinations of tensile, compressive, and torsional mean and alternating stresses on fatigue life. He reported that alternating shear stresses appeared to cause fatigue failure. On this basis, he formulated a criterion including the amplitude of octahedral shear stresses and the first linear stress invariant. The stress components of these criteria are easy to obtain from FEA's. The invariant formulae usually consist of quantities related to hydrostatic and octahedral stresses. The use of these hypotheses allows to determine the initiation point of fatigue cracks provided that structural load conditions respect two main assumptions:

- the structure is subject to alternating proportional loads;
- the directions of the principal stresses are fixed during the application of the loads.

However, the orientation of potential cracks with these criteria cannot be defined.
The Sines criterion has the following form:

$$\tau_{oct} + k\sigma_{H,m} \leq \lambda \tag{1}$$

The first term on the left-hand side of Eq. (1) is the octahedral shear stress, τ_{oct}:

$$\tau_{oct} = \frac{\sqrt{2}}{3}\sqrt{\sigma_{1,a}^2 + \sigma_{2,a}^2 + \sigma_{3,a}^2 - (\sigma_{1,a}\sigma_{2,a} + \sigma_{1,a}\sigma_{3,a} + \sigma_{2,a}\sigma_{3,a})} \tag{2}$$

where σ_1, σ_2 and σ_3 are the amplitudes of the alternating principle stresses.
The second term on the left-hand side of Eq. (1) is a hydrostatic stress term, $\sigma_{H,m}$:

$$\sigma_{H,m} = \left(\frac{\sigma_{1,m} + \sigma_{2,m} + \sigma_{3,m}}{3}\right) \tag{3}$$

where $\sigma_{1,m}$, $\sigma_{2,m}$ and $\sigma_{3,m}$ are the amplitudes of the mean principle stresses;
λ = is material constant proportional to reversed fatigue strength;
k = is a numerical material constant, which gives variation of the permissible range connected to the hydrostatic stress.
The constants λ and k may be easily determined from fatigue tests with a large R-ratio difference. For example, in a fully reversed uniaxial test (R-ratio = -1), Eq. (1) gives:

$$\frac{\sqrt{2}}{3}\sigma_{1,a} = \lambda$$

letting $\sigma_{1,a} = \sigma_{f,a}$ it is obtained:

$$\lambda = \frac{\sqrt{2}}{3}\sigma_{f,a}$$

where $\sigma_{f,a}$ is the amplitude of reversed axial stress that would cause failure at the desired cyclic load. For pulsating load from 0 to $\sigma_{\max}$ (R-ratio = 0) it is obtained:

$$\sigma_{1,a} = \sigma_{1,m}$$

and Eq. (1) may become:

$$\frac{\sqrt{2}}{3}\sigma_{1,a} = \lambda - \frac{1}{3}k\sigma_{1,m}$$

Letting $\sigma_{1,a} = \sigma_{p,a}$ it is obtained:

$$k = \sqrt{2}\left(\frac{\sigma_{f,a}}{\sigma_{p,a}} - 1\right)$$

where $\sigma_{p,a}$ is the amplitude of fluctuating stress that would cause failure at the same cyclic life as $\sigma_{f,a}$.
For computer calculations, a convenient notation introduces the von Mises equivalent stress so the Sines criterion Eq. (1) becomes:

$$\sigma_{eq,a(vonMises)} + \left(\frac{\sigma_{f,a}}{\sigma_{p,a}} - 1\right)\cdot\left(\sigma_{1,m} + \sigma_{2,m} + \sigma_{3,m}\right) \le \sigma_{f,a} \tag{5}$$

For the numerical implementation of the criteria, the scripting language of the FE code ANSYS® , that is the Ansys Parametric Design Language (APDL), was used. APDL makes possible to record current values of the stress tensor components and a certain predefined quantity (e.g., equivalent stresses). The fatigue analysis programs the Sines criterion, containing two series of static calculations: for equivalent average and amplitude loads. From the FE analysis, the invariants (i.e. the criterion components) were obtained in the whole structure.
The algorithm ran four times: in each run, the aforementioned fatigue strengths were set to evaluate a fatigue life respectively of 10^4, 10^5, 10^6 and 10^7 cycles. A fifth run was performed at the failure cycle number (177˙000). The fatigue strengths were collected from the Haigh diagrams for the considered materials. Tab. 2 summarizes the fatigue limits that define the Haigh diagram for each number of cycles.

Material	10^4 Cycles		10^5 Cycles		$1.77 \cdot 10^5$ Cycles		10^6 Cycles		10^7 Cycles	
	$\sigma_{f,a}$ [MPa]	$\sigma_{p,a}$ [MPa]	$\sigma_{f,a}$ [MPa]	$\sigma_{p,a}$ [MPa]	$\sigma_{f,a}$ [MPa]	$\sigma_{p,a}$ [MPa]	$\sigma_{f,a}$ [MPa]	$\sigma_{p,a}$ [MPa]	$\sigma_{f,a}$ [MPa]	$\sigma_{p,a}$ [MPa]
Al2024 T3	341	214	238	166	225	162	162	124	138	110
Al7075 T6	345	286	222	224	236	183	179	172	155	145

Table 2: Fatigue properties of the materials [30].

RESULTS AND DISCUSSION

Static testing

Figs. 10-15 plot the maximum principal strains for the three static loading configurations analysed (T1–T3). Numerical strains, provided along the strain gages directions, are compared with the corresponding experimental data in Tabs. 3-5. With static loading configuration (T1) the numerical results are in good agreement with the values of strain gages, located on the skin (i.e. less than 8.5 % relative difference), while with reference to the strain gages S3 and S5, that are on the top of the frames, the results are affected to secondary bending effects.
Moreover it is interesting to highlight that the best correlations are obtained when considering a biaxial load (T3) because the former condition involves the lowest secondary bending effects and the worst with a uniaxial loading along the stringer direction (T2) because the local secondary bending is non negligible with the presence of local bulging effects and the consequent need for a more complex three dimensional modelling.

Strain gages	Uniaxial loading along frame direction (T1 test) P_y = 400 kN		
	FEM strain (a) [μm/m]	Experimental strain (b) [μm/m]	Deviation = (a-b)*100/b [%]
S1	-389	-419	-7.7
S2	1311	1354	-3.2
S3	842	1260	-33.2
S4	1634	1673	-2.3
S5	837	1126	-25.7
S6	1275	1245	2.4
S7	-371	-405	-8.4

Table 3: Numerical and experimental correlation for load configuration T1.

Strain gages	Uniaxial loading along stringer direction (T2 test) P_x = 250 kN		
	FEM strain (a) [μm/m]	Experimental strain (b) [μm/m]	Deviation = (a-b)*100/b [%]
S1	710	692	2.6
S2	-182	-368	-50.5
S3	-249	-273	-8.8
S4	-266	-513	-48.1
S5	-245	-231	6.1
S6	-167	-321	-47.9
S7	711	681	4.4

Table 4: Numerical and experimental correlation for load configuration T2.

Strain gages	Biaxial loading (T3 test) P_y = 400 kN, P_x = 250 kN		
	FEM strain (a) [μm/m]	Experimental strain (b) [μm/m]	Deviation = (a-b)*100/b [%]
S1	267	255	4.7
S2	1136	1117	1.7
S3	1117	1074	4.0
S4	1391	1394	-0.2
S5	1103	1051	9.5
S6	1038	1048	-0.9
S7	291	270	7.7

Table 5: Numerical and experimental correlation for load configuration T3.

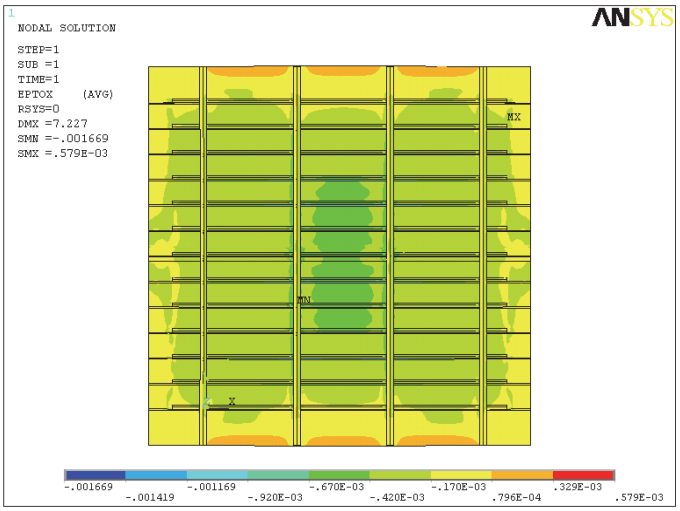

Figure 10: ε_x strain for load configuration T1.

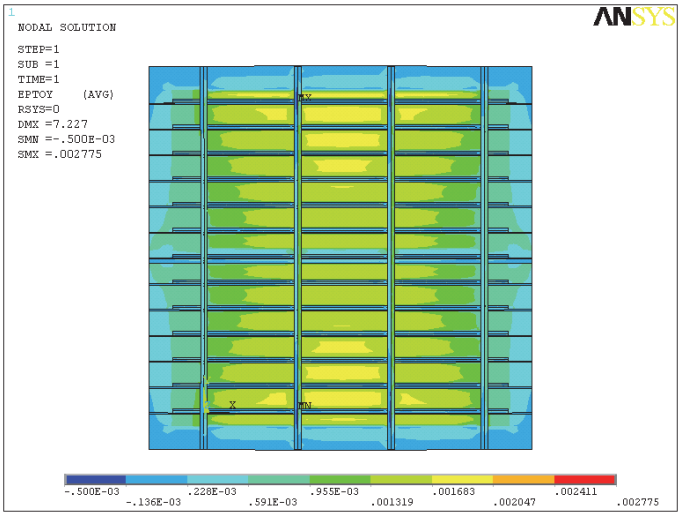

Figure 11: ε_y strain for load configuration T1.

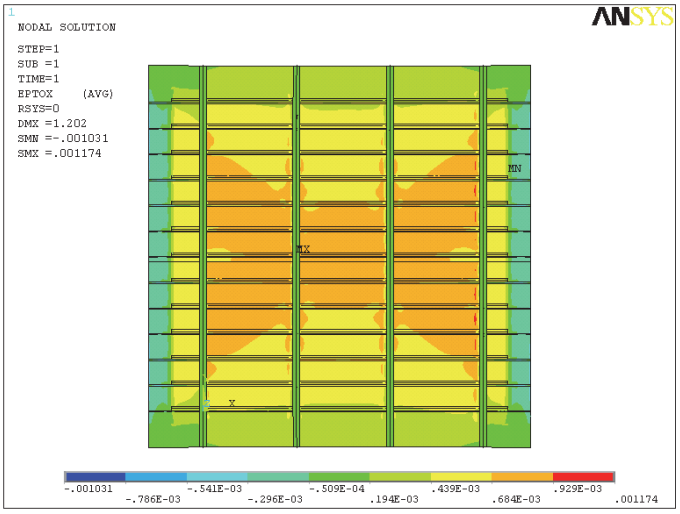

Figure 12: ε_x strain for load configuration T2.

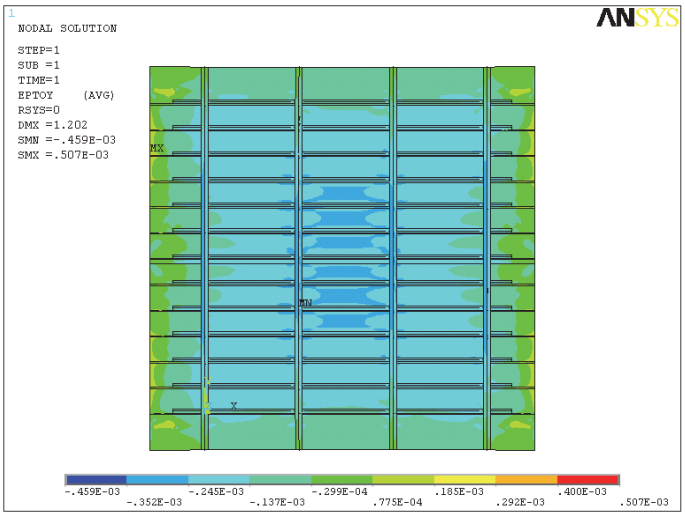

Figure 13: ε_y strain for load configuration T2.

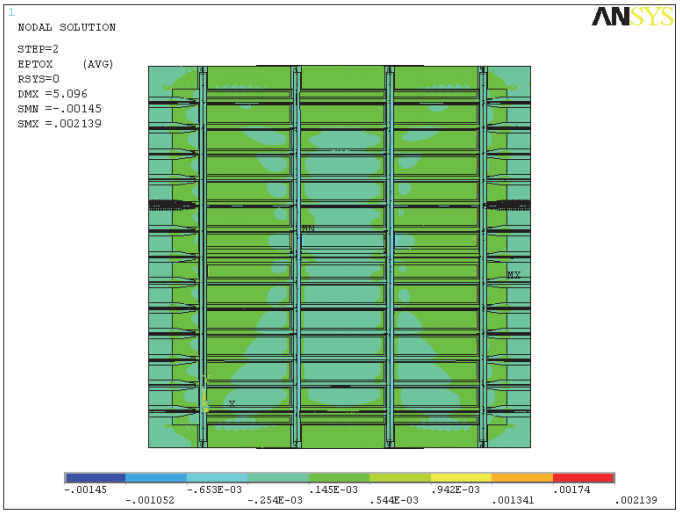

Figure 14: ε_x strain for load configuration T3.

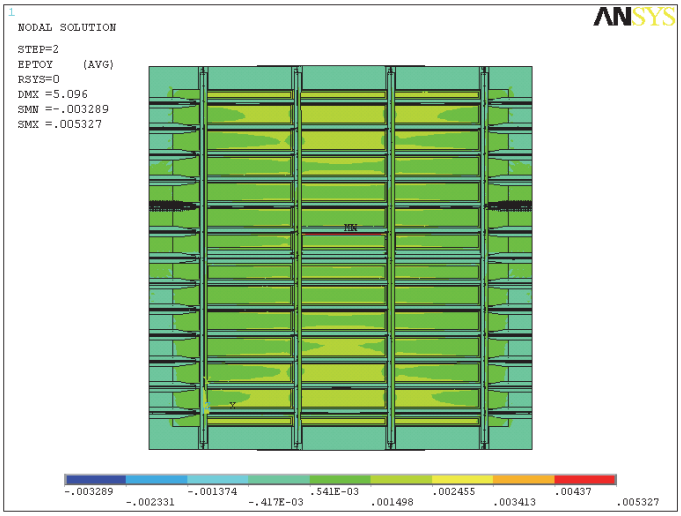

Figure 15: ε_y strain for load configuration T3.

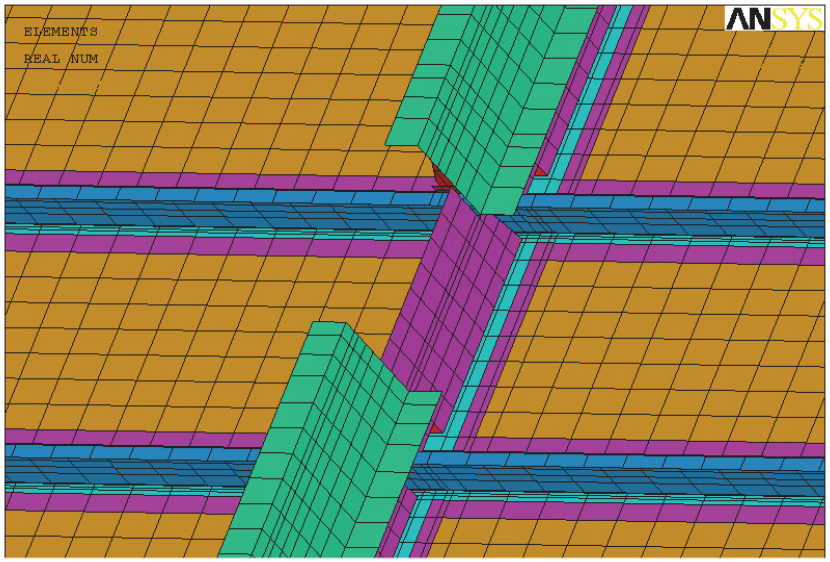

Figure 16: FE model of the panel.

To simulate the effect of the breakage of the frame, another FE model of the panel has been developed. In this model the frame in the failure zone was not modeled. In Fig. 16 the panel zone is shown with the broken frame.
In Tab. 6 some values of measured strains corresponding to a load applied along the frame direction (P_y = 400 kN) and the corresponding numerical ones, expressed with the relative deviation, are reported. The numerical results are in good agreement with the experimental results, the higher deviation of the strain gauge S3 is due to the secondary bending.

Strain gages	Uniaxial load along frame direction (T1 test) P_y = 400 kN		
	FEM strain (a) [μm/m]	Experimental strain (b) [μm/m]	Deviation = (a-b)*100/b [%]
S1	-389	-460	7.7
S2	1312	1399	-6.2
S3	848	1305	-35.0
S4	1697	1727	1.7
S5	-	-	-
S6	1317	1285	2.6
S7	-406	-420	3.2

Table 6: Numerical and experimental correlation for load configuration T1 for panel with broken frame.

Fatigue testing

The results of conducted fatigue analysis of the fuselage panel are presented in form of contour plot of the ratio:

$$\rho = \left[\sigma_{eq,a(vonMises)} + \left(\frac{\sigma_{f,a}}{\sigma_{p,a}} - 1 \right) \cdot \left(\sigma_{1,m} + \sigma_{2,m} + \sigma_{3,m} \right) \right] / \sigma_{f,a} \tag{6}$$

accordingly to the investigated criteria.
The values equal or greater than 1 are indicative of critical points; the higher the value, the higher the possibility of failure. Values less than 1 are typical of locations that are not critical fatigue-wise.
The resulting contour plots presents a consistent pattern, showing that the highest Sines ratio is always located at the bottom of the panel (marked by a circle in Figs. 17-21), near the third frame, on the rear side. As shown in Fig. 17, there are no critical points after 10˙000 cycles (r_{max} = 0.8); critical zones begin to appear just before 100˙000 cycles (r_{max} = 1.015) (Fig. 18). The extension of the critical zones increases at the locations near the lower bay, extending along the lower stringer. As the number of cycles goes up, more zones interested by the fatigue critical condition appear on the left side of the panel (Figs. 19-21). At 177˙000 cycles (Fig. 19) numerical results predict panel failure at an applied load level 1.033 times the experimental one.

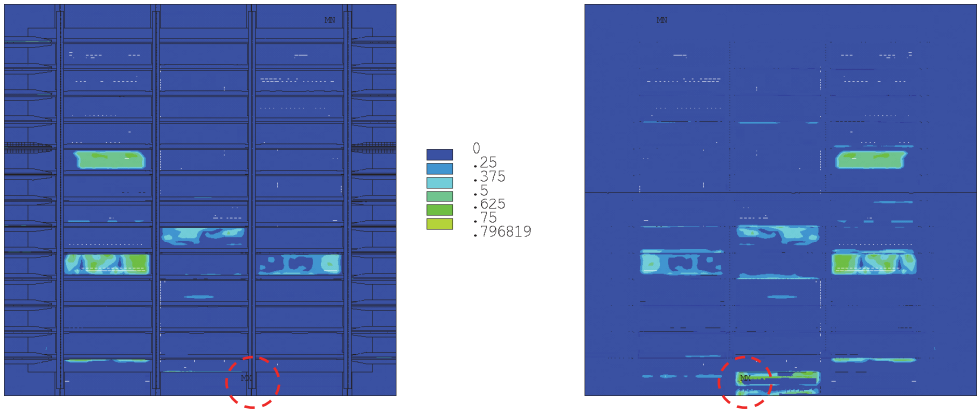

Figure 17: ρ values after 10^4 cycles: front (left) and rear (right) sides.

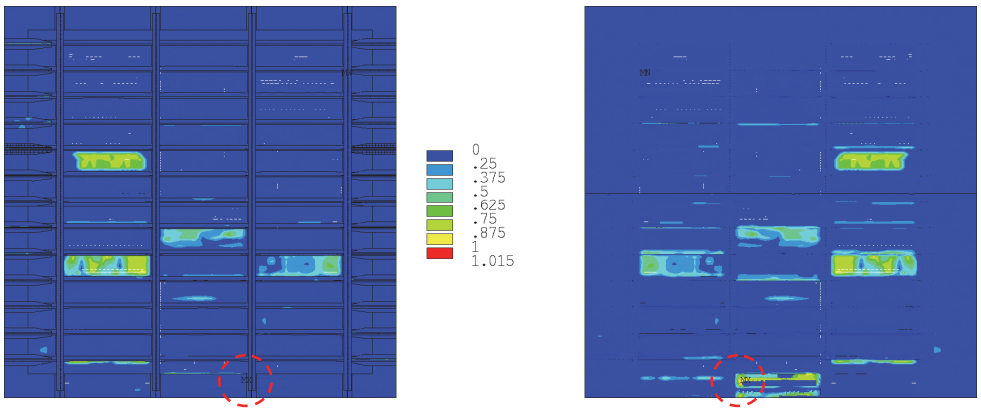

Figure 18: ϱ values after 10^5 cycles: front (left) and rear (right) sides.

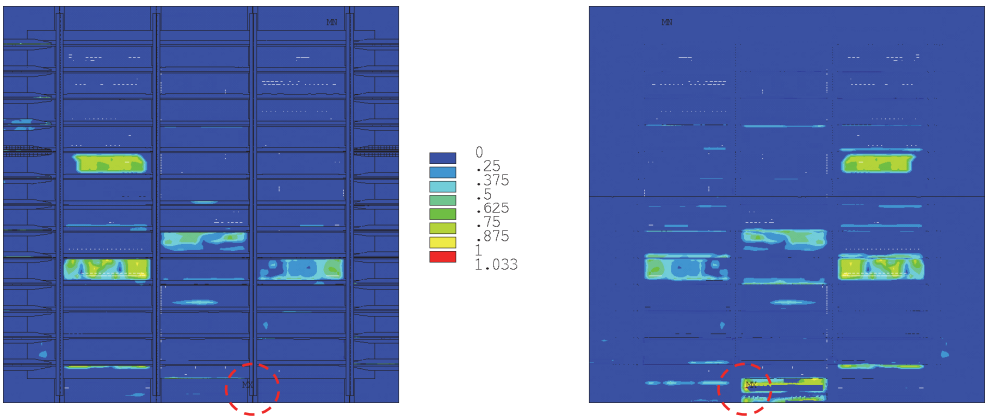

Figure 19: ϱ values after $1.77 \cdot 10^5$ cycles: front (left) and rear (right) sides.

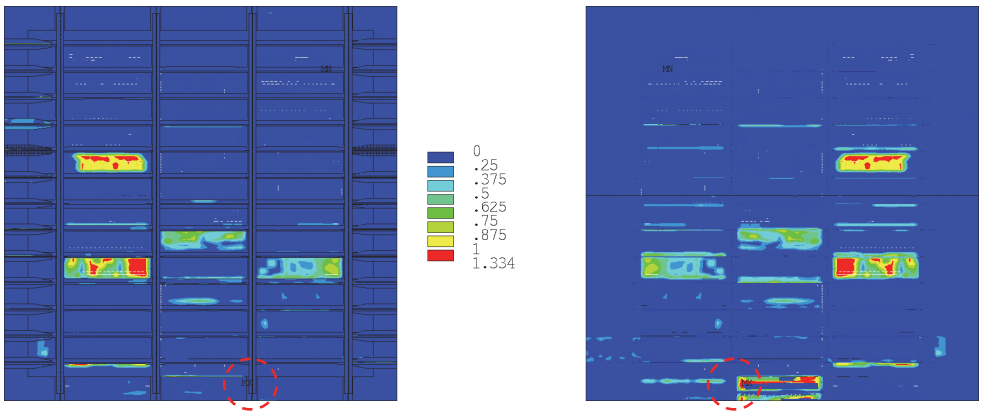

Figure 20: ϱ values after 10^6 cycles: front (left) and rear (right) sides.

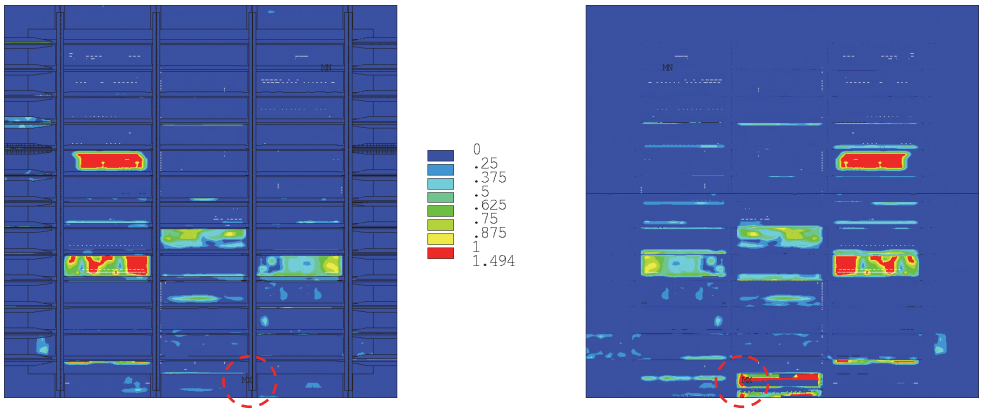

Figure 21: ϱ values after 10^7 cycles: front (left) and rear (right) sides.

In Fig. 22 are highlighted the failure zone at 177,000 cycles. It is interesting to observe how the numerical analyses are able to predict the failure zone.

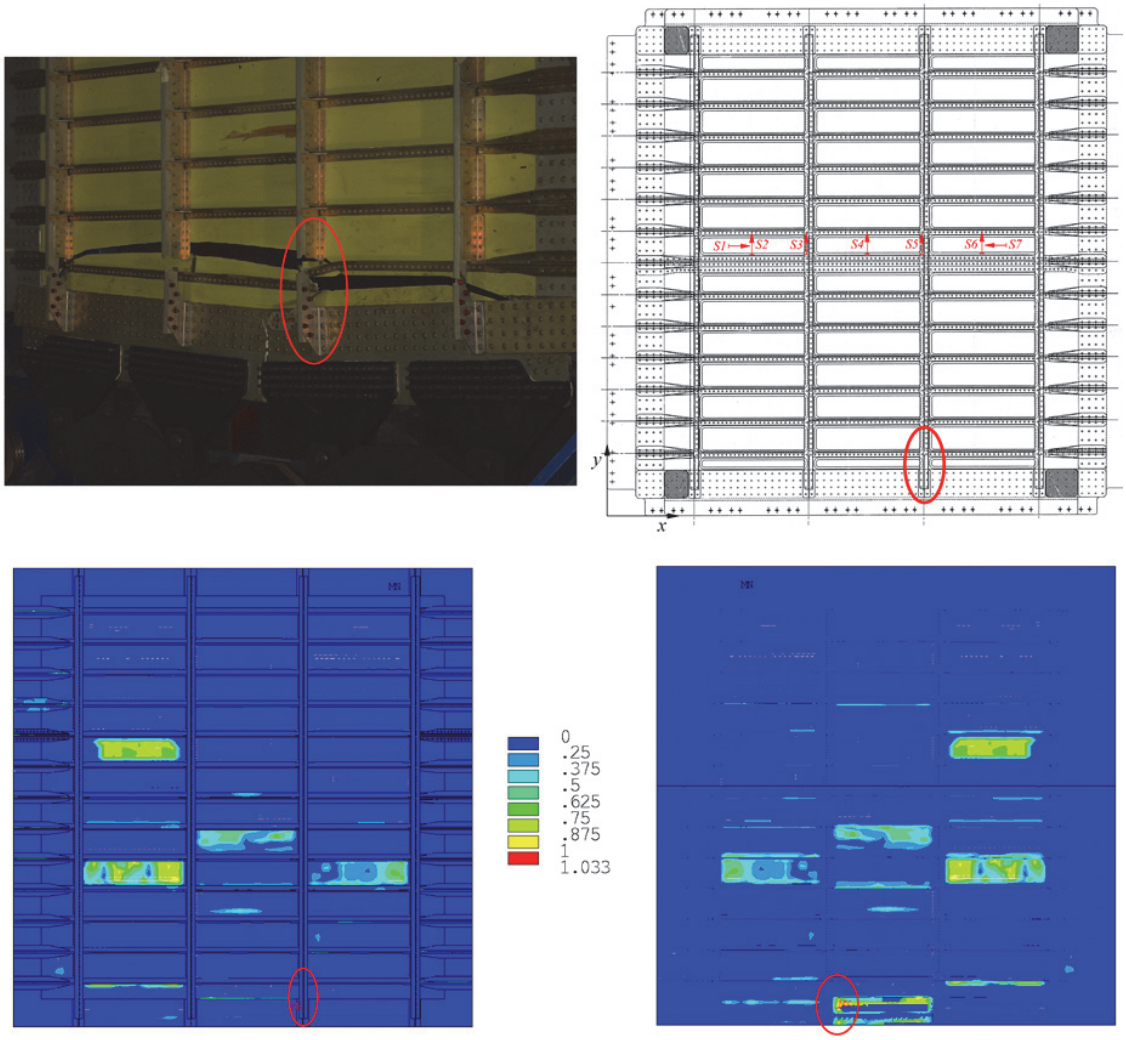

Figure 22: Final failure at 177000 cycles and numerical results comparison.

CONCLUSIONS

The development of reliable methods to predict the damage tolerant behaviour is helpful for the designer to achieve more and more efficient structures. In this work static and fatigue tests on a full scale fuselage panel were carried out. After 177˙000 cycles the panel broke down at the middle-lower bay, near the third frame. The experimental results were useful in the assessment of the accuracy of the numerical FE model when determining the critical area. With reference to the static test, the correlation between numerical and experimental results is judged satisfactory, because the strain differences are comparable to the intrinsic error level inherent the strain gauge usage for most of strain gauges; numerical higher errors are expected in those zones where the allowance for geometry and stress field complexity is not provided due to the simplifications related to the two dimensional numerical approach.
The results of the numerical analyses are in good agreement with the experimental analysis data collected by the tests on the full scale panel: the latter broke due to fatigue after 177˙000 cycles, while the model had predicted the initiation of the fatigue crisis at about 100˙000 cycles. At 177˙000 cycles the difference between numerical evaluation of the critical fatigue load and experimental data may be determined in terms of 3.3%. The position of the failure is predicted approximately in the same zone, located on the skin. Overall, these results show that the Sines criterion can be an effective method to rapidly evaluate the initiation of fatigue crisis. The method hereby proposed has the additional advantage of providing, with a single analysis, a description that is both qualitative and quantitative of the fatigue status of the structure. A rather good correlation was obtained between numerical results and experimental data in static loading conditions.

REFERENCES

[1] Molent, L., Barter, S.A., A comparison of crack growth behaviour in several full-scale airframe fatigue tests, Int. J. Fatigue, 29 (6) (2007) 1090-1099.
[2] Wang, S.S., Chu, R.C., Full scale fatigue crack growth test of advanced jet trainer AT-3, Theor. Appl. Fract. Mec., 11 (2) (1989) 71-91.
[3] Sepe, R., Armentani, E., Caputo, F., Lamanna, G., Fatigue behaviour of full scale flat stiffened aeronautic panels, Key. Eng. Mat., 627 (2015) 97-100.
[4] Giglio, M., Manes, A., Crack propagation on helicopter panel: Experimental test and analysis, Eng. Fracture Mechanics, 75 (3-4) (2008) 866-879.
[5] Armentani, E., Citarella, R., Sepe, R., FML Full Scale Aeronautic Panel Under Multiaxial Fatigue: Experimental Test and DBEM Simulation, Eng. Fract. Mech., 78 (8) (2011) 1717-1728.
[6] Cordes, J.A., Predicting the fatigue cycles on aluminum panels, Int. J. Fatigue, 23 (1) (2001) 5-12.
[7] Grbovic, A., Rasuo, B., FEM based fatigue crack growth predictions for spar of light aircraft under variable amplitude loading, Eng. Fail. Anal., 26 (2012) 50-64.
[8] Šedek, J., Růžek, R., Raška, J., Běhal, J., Comparative study of prediction methods for fatigue life evaluation of an integral skin-stringer panel under variable amplitude loading, Procedia Eng., 114 (2015) 124-131.
[9] Furukawa, C.H., Bucalem, M.L., Mazella, I.J.G., On the finite element modeling of fatigue crack growth in pressurized cylindrical shells, Int. J. Fatigue, 31 (4) (2009) 629-635.
[10] Citarella, R., Perrella, M., Multiple surface crack propagation: numerical simulations and experimental tests, Fatigue Fract. Eng. M., 28 (2005), 135-148.
[11] Citarella, R., Cricrì, G., A two-parameter model for crack growth simulation by combined FEM-DBEM approach, Adv. Eng. Softw., 40 (5) (2009) 363-377.
[12] Sepe, R., Armentani, E., Di Lascio, P., Citarella, R., Crack Growth Behavior of Welded Stiffened Panel, Procedia Engineering, 109 (2015) 473-483.
[13] Citarella, R., Non Linear MSD crack growth by DBEM for a riveted aeronautic reinforcement, Adv. Eng. Softw., 40 (4) (2009) 253-259.
[14] Citarella, R., MSD Crack propagation on a repaired aeronautic panel by DBEM, Adv. Eng. Softw., 42 (10) (2011) 887-901.
[15] Armentani, E., Citarella, R., DBEM and FEM analysis on non-linear multiple crack propagation in an aeronautic doubler-skin assembly, Int. J. Fatigue, 28 (5-6) (2006) 598–608.
[16] Romeo, G., Frulla, G., Buckling of simply supported and clamped anisotropic plates under combined loads, Spacecraft Structure and Mechanical Testing, Noordwijk, The Netherlands, (1991).

[17] Cricrì, G., Perrella, M., Calì, C., Experimental and Numerical Post-buckling Analysis of Thin Aluminium Aeronautical Panels under Shear Load, Strain, 50 (2014) 208-222.
[18] Calì, C., Castellano, C., Godono, G., Analysis of operative conditions of a machine for buckling tests in compression or shear of ortotropic cylindrical panels, Italian-Polish Meeting on Analisi e Controllo dei Sistemi Complessi, Naples, Italy (1992).
[19] Boehler, J.P., Demmerle, S., Koss, S., A New Direct Biaxial Testing Machine for Anisotropic Materials, Exp. Mech., 34 (1) (1994) 1-9.
[20] Sonsino, C.M., Multiaxial fatigue of welded joints under in-phase and out of- phase local strains and stresses. Int J Fatigue, 17 (1) (1995) 55-70.
[21] Sonsino, C.M., Influence of load and deformation-controlled multiaxial tests on fatigue life to crack initiation, Int J Fatigue, 23 (1) (2001) 159-167.
[22] Backstrom, M., Marquis, G., A review of multiaxial fatigue of weldments: experimental results, design code and critical plane approaches, Fatigue Fract. Eng. Mater. Struct, 24 (2001) 279-291.
[23] Gómez, C., Canales, M., Calvo, S., Rivera, R., Valdés, J.R., Núñez, J.L., High and low cycle fatigue life estimation of welding steel under constant amplitude loading: Analysis of different multiaxial damage models and in-phase and out-of-phase loading effects, Int. J. Fatigue, 33 (4) (2011) 578-587.
[24] Dang Van, K., Griveau, B., Message, O., On a new multiaxial fatigue limit criterion: theory and application, biaxial and multiaxial fatigue, EGF 3. Mechanical Engineering Publications, London, (1989) 479-496.
[25] Fatemi, A., Shamsaei, N., Multiaxial fatigue: An overview and some approximation models for life estimation, Int. J. Fatigue, 33 (8) (2011) 948-958.
[26] Wang, Y., Yao, W., Evaluation and comparison of several multiaxial fatigue criteria, Int. J. Fatigue, 26 (1) (2004) 17-25.
[27] Fatemi, A., Socie, D.F., A critical plane approach to multiaxial fatigue damage including out-of-phase loading, Fatigue Fract. Eng. Mater. Struct., 11 (1988) 149-165.
[28] Fatemi, A., Kurath, P.P., Multiaxial fatigue life prediction under the influence of mean stresses, ASME J. Eng. Mater. Technol., 110 (1988) 380-388.
[29] Sines, G., Behaviour of metals under complex static and alternating stresses, in 'metal fatigue'. McGraw-Hill, New York, (1959) 145-169.
[30] Buch, A., Fatigue Strength Calculation, Trans Tech Publications, Switzerland, (1988).